Nat. Hazards Earth Syst. Sci., 6, 303–314, 2006
www.nat-hazards-earth-syst-sci.net/6/303/2006/

Natural Hazards and Earth System Sciences

Statistical analysis and modelling of weather radar beam propagation conditions in the Po Valley (Italy)

A. Fornasiero[1,2], **P. P. Alberoni**[1], **and J. Bech**[3,4]

[1]Servizio IdroMeteorologico, A. R. P. A. Emilia Romagna, Viale Silvani, 6, 40 122 Bologna, Italy
[2]Centro di ricerca Interuniversitario in Monitoraggio Ambientale, Polo Accademico Savonese, Via Cadorna 7, 17 100 Savona, Italy
[3]Servei Meteorològic de Catalunya, Berlín 38, 08 029 Barcelona, Spain
[4]Departament d'Astronomia i Meteorologia, Universitat de Barcelona, Martí i Franqués, 1, 08 028 Barcelona, Spain

Received: 28 October 2005 – Revised: 7 February 2006 – Accepted: 13 February 2006 – Published: 8 May 2006

Abstract. Ground clutter caused by anomalous propagation (anaprop) can affect seriously radar rain rate estimates, particularly in fully automatic radar processing systems, and, if not filtered, can produce frequent false alarms. A statistical study of anomalous propagation detected from two operational C-band radars in the northern Italian region of Emilia Romagna is discussed, paying particular attention to its diurnal and seasonal variability. The analysis shows a high incidence of anaprop in summer, mainly in the morning and evening, due to the humid and hot summer climate of the Po Valley, particularly in the coastal zone. Thereafter, a comparison between different techniques and datasets to retrieve the vertical profile of the refractive index gradient in the boundary layer is also presented. In particular, their capability to detect anomalous propagation conditions is compared. Furthermore, beam path trajectories are simulated using a multilayer ray-tracing model and the influence of the propagation conditions on the beam trajectory and shape is examined. High resolution radiosounding data are identified as the best available dataset to reproduce accurately the local propagation conditions, while lower resolution standard TEMP data suffers from interpolation degradation and Numerical Weather Prediction model data (Lokal Model) are able to retrieve a tendency to superrefraction but not to detect ducting conditions. Observing the ray tracing of the centre, lower and upper limits of the radar antenna 3-dB half-power main beam lobe it is concluded that ducting layers produce a change in the measured volume and in the power distribution that can lead to an additional error in the reflectivity estimate and, subsequently, in the estimated rainfall rate.

Correspondence to: P. P. Alberoni
(palberoni@arpa.emr.it)

1 Introduction

Anomalous propagation of weather radar beams occurs when the atmospheric thermodynamic vertical structure produces a refractivity gradient value outside its normal range. This range is associated to the so-called standard conditions, i.e. a distribution of temperature, pressure and humidity, representative of the average atmosphere at mid–latitudes. In the first kilometres of the atmosphere, the gradient ranges normally between 0 and $-79\,\mathrm{km}^{-1}$ and its mean value at mid–latitudes is approximately $-40\,\mathrm{km}^{-1}$ (Doviak and Zrnic, 1993). Within these standard propagation conditions microwaves are bent slightly downward from a straight line given by the original antenna direction. Above the upper limit subrefraction occurs (i.e. beams are less refracted), with a consequent greater increase of the beam height with the distance and a reduction of the maximum effective detection range (i.e. the radar beam overshoots the precipitation more easily); below the lower threshold superrefraction occurs, which implies a lower increase of the height with the distance and an increase in the maximum observable range. If the refractivity gradient is below $-157\,\mathrm{km}^{-1}$ then ducting conditions are present and an initially horizontal beam propagates towards the earth surface. In this case, the ground reflects part of the power and this produces a strong non-meteorological echo. It should be noted that ducting occurrence also requires a minimum incidence angle between the radar beam and the ducting layer (ITU, 1997). In practice, this means that only the lowest antenna elevation angles are usually affected by anomalous propagation.

In fully automated radar processing systems, anomalous propagation can produce frequent false alarms of intense rainfall rates. Moskowicz et al. (1994) showed how, for an anaprop event, the local rain accumulation maxima were about four times higher than for heavy rainfall; they indicated too the amount of anaprop contribution in the accumulated

Published by Copernicus GmbH on behalf of the European Geosciences Union.

precipitation over Poland in 1991 reached 59% in June and 97% in September. Such errors may compromise totally the radar rainfall estimate. Superrefraction is produced at interfaces between cool-humid and warmer-dryer layers, i.e. with temperature inversions and/or humidity decrease. Meteorological conditions leading to this occurrence are (Skolnik, 2001; Raghavan, 2003):

1. Nocturnal radiative cooling: when the ground is humid and cool and the upper air is warm (air has a lower thermal capacity than water). It is frequent in the Po Valley, mainly in July and August (Alberoni et al., 1998):
2. Advection of warm and dry air over the sea (land breeze) or of humid and cool air over the land (sea breeze).
3. Water evaporation at sea surface (evaporation duct).
4. Down drift of humid and cool air during thunderstorms.
5. Subsidence of warm and dry air in presence of high pressures cells, over moist layers.

In these cases the radar signal can be "trapped": the phenomenon is distinguished between surface ducting and elevated ducting, respectively, if the bottom of the duct is on the ground or above it at a few hundred meters. Bech et al. (2002) found that, over the Barcelona area (NE Spain), the bottom layer of the first elevated duct oscillated between 700 m and 1500 m. Previous statistical studies, obtained analysing radiosounding data, showed that the highest incidence of anaprop events (with superrefraction) is in summer and during the night as quoted by Babin (1996), Alberoni et al. (2001) and Bech et al. (2002). On the other hand, subrefraction can occur in presence of rain, when high humidity is present up to high altitudes (Raghavan, 2003) or with fog (Skolnik, 2001).

The recognition of anomalous propagation conditions and the precise determination of the beam path is an important aim in some meteorological applications, such as topographic beam blocking estimates (Bech et al., 2003), data assimilation and in general of the quality control of radar data (Alberoni et al., 2003). It requires an accurate description of the refractivity index gradient profile, a quantity that can be retrieved using radiosounding data or, more precisely, using refractometers (Skolnik, 2001). The second way is more expensive and requires the use of a helicopter to measure at different heights. Radiosonde observations are cheaper but usually they are available, in most stations, only every twelve hours. Moreover, the common format of data exchange (TEMP data) may limit drastically the vertical resolution missing some anaprop features. A possible solution to improve the temporal–and spatial–resolution of radiosonde data is the use of numerical weather prediction (NWP) models. Bech et al. (2004) compared the output of a hydrostatic NWP model (the MASS model) with radiosounding observations. They found that the model tended to underestimate superrefraction though forecasts could be improved significantly if combined with previous radiosonde observations.

The aim of the present work is to assess the statistical characteristics of the propagation condition in the eastern part of the Po Valley; a second scope is to verify the capability of TEMP data and of the Lokal Model (version 2.19) to reproduce propagation conditions, even in order to assess the usefulness of this model data to fill temporal gaps in the observations. The Lokal Model is a non hydrostatic NWP model developed by the German weather service (Doms and Schaettler, 1999), and improved and maintained in collaboration with the Cosmo consortium, participated by the Emilia-Romagna regional meteorological service. Particular efforts have been devoted to describe the effects of anomalous propagation on beam shape and power distribution and how these effects are reproduced from the different datasets.

2 A brief review of radar signal propagation theory

In the low troposphere electromagnetic waves do not propagate generally in a straight line; its path is a curve depending on the variation of the refractive index n, which is (in the troposphere) a function of the temperature and water content. Empirical observations demonstrate that the refractive index gradient, in standard conditions and in the first 2 km of the atmosphere, is constant and inversely proportional to the earth radius. In this case the effective earth radius (hypothetic radius that the earth should have, considering the ray path as a straight line, to keep the relation between ray height and arc length) is:

$$a_e = 4/3 \times a \tag{1}$$

where a is the earth radius and a_e is the effective earth radius. Usually, instead of the refractive index n, it is convenient to describe propagation conditions with an associated magnitude, the refractivity N (where $N=(n-1)\times 10^6$). For microwaves and in the low troposphere, this value can be estimated through the formula of Bean and Dutton (1968), with an accuracy of 0.1:

$$N = (77.6/T)/(P + 4810 P_w/T) \tag{2}$$

where N, the refractivity, is an adimensional number, P is the total pressure (hPa), P_w is the partial pressure of water vapour (hPa) and T is the temperature (K). In the first kilometres of the atmosphere the temperature decreases generally with height and in standard conditions, the N gradient is near $-40\,\mathrm{km}^{-1}$. In temperature inversion conditions, this value is often lower than $-157\,\mathrm{km}^{-1}$and the ray could be bent up to hit the ground. Furthermore, the propagation depends strongly on local thermodynamic conditions, which vary substantially in space and time. Anaprop events are generally determined from the thermodynamic conditions of the

first 200–300 m of atmosphere. In flat land the radar beam reaches this height above ground at relatively short ranges; therefore, even if a co-located sounding station is unable to describe exactly the propagation conditions over the whole radar domain, radiosonde data can help to recognize anaprop conditions in flat land.

Once the N gradient is known, the height h relative to the earth of a radar wave can be calculated through the following formula (refer to Doviak and Zrnic, 1993).

$$h = \sqrt{r^2 + (k_e a)^2 + 2rk_e a \sin\theta} - k_e a + H_0 \quad (3)$$

where r is the distance from radar, a the Earth's radius, θ the antenna elevation angle and H_0 the antenna's height; where $k_e$is a factor dependent on N, that, multiplied by a (Earth's radius) gives the effective Earth's radius. This formula neglects horizontal variations of the refractivity gradient, its application allows to perform "ray tracing" (Skolnik, 2001), i.e. a simplified description of the radar beam trajectories based on a geometric optics approach. A more complete beam path and power distribution description is given by the parabolic equation model, which takes into account the three-dimensional refractivity field, but requires a large computational effort (Bebbington, 1998). In this study the computation of exact power distribution is not needed therefore the geometric approach, described in detail in Sect. 5, has been adopted.

3 The San Pietro Capofiume and Gattatico radar: statistics of anomalous propagation

In this section a description of the statistics of anomalous propagation (superrefraction) occurrence is presented, based on a texture analysis of the reflectivity data from San Pietro Capofiume and Gattatico radar.

The San Pietro Capofiume and Gattatico radars (hereinafter SPC and GAT) are dual-polarization systems. Each one is placed on a tower with a Cassegrain parabolic antenna without radome cover, providing a half-power beam-width of 0.9° and a directivity of about 46 dB. Including the tower height, SPC antenna is at 31 m a.s.l., while GAT antenna is at 66 m a.s.l. The klystron peak-power is 500 kW at 5.6 GHz with an alternating horizontal-vertical polarization transmission and dual pulse repetition frequency (PRF) system to allow radial velocity unfolding capability. Pulse widths of 0.5 μs (i.e., short pulse with a resampled bin resolution of 250 m) and 1.5 μs (i.e., medium pulse with a resampled bin resolution of 1000 m). The receiver sensitivity is of the order of -113 dBm, depending of the selected pulse. The maximum ranges used are typically 250 km (with medium pulse) and 125 km (with short pulse).

The two systems are located in Emilia-Romagna region, (northern Italy) in the Po valley (refer to Fig. 1a). GAT is nearer to the West side of Appennino and its minimum coverage includes a large mountainous area. SPC is located at

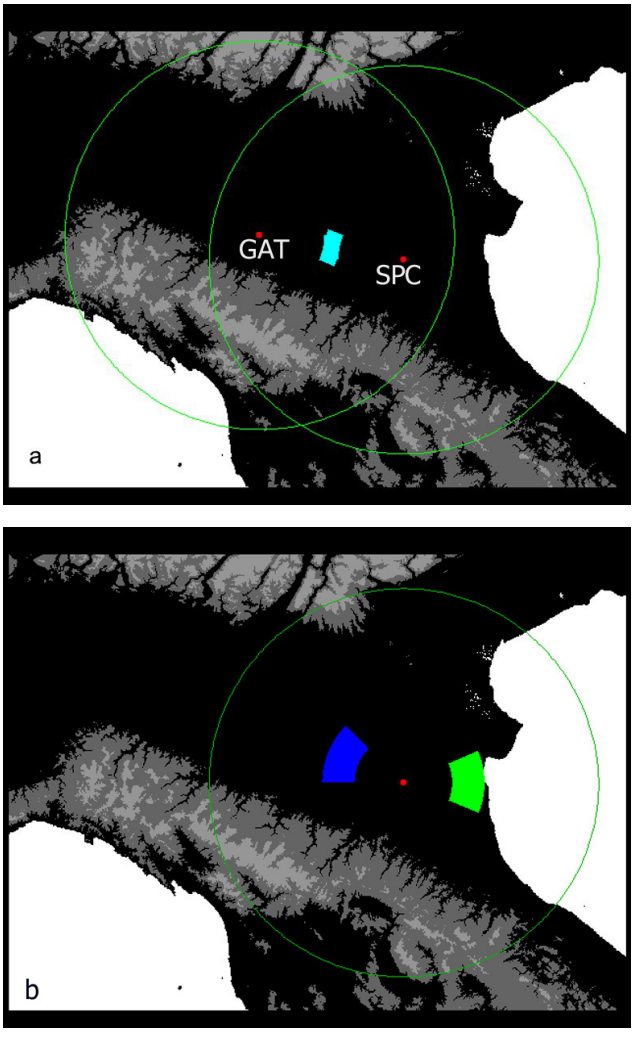

Fig. 1. Map of Northern Italy indicating the radars used in the analysis: San Pietro Capofiume (SPC) and Gattatico (GAT). **(a)** common cell of GAT and SPC radars (in blue) **(b)** costal (green) and inland (blue) boxes.

60 km from the East coast of Italy, covering a large flat land and sea area. Medium pulse data are operationally decluttered through static map and using an algorithm of anaprop detection (Alberoni et al., 2001); short pulse data is first processed with a Doppler filter and then the anaprop algorithm is applied.

A previous study on the same area (Alberoni et al., 1998) was carried out computing the climatology of the refractive index, using four years of radiosonde data at 00:00 UTC and 12:00 UTC, from the sounding station co-located at San Pietro Capofiume radar station. Accordingly with the propagation condition anaprop was defined when a refractivity gradient lower than -157 km^{-1} in the first 50 m of atmosphere was present. They found out that the highest anaprop incidence occurs at midnight with a frequency of 61% (respect to the 22% at noon time) and in summer season when

the midnight incidence is approximately 80% respect to 53% of midday.

A limitation of the previous study is due to the temporal spacing between two subsequent observations, indeed, as usual for soundings, data are available only twice a day. In order to study the seasonal and diurnal cycle of anaprop echoes, a detection algorithm that calculated the percentage of radar pixels affected by anomalous propagation throughout the day, was used (Alberoni et al., 2001). In order to assess the impact of these phenomena, it was used the short pulse dataset, which, as previously stated, was already decluttered with a Doppler filter. The detection algorithm tested the vertical continuity of the reflectivity value: if the difference between the reflectivity of two adjacent range bins or cells (at consecutive elevations) was higher than a given threshold, then the pixel was recognized as clutter. The first elevation considered for each cell was derived from the static map obtained during fine weather and normal propagation days: it indicated, for each cell, the first elevation not affected from clutter during normal conditions. This lead to classify the recognized clutter as due to anomalous propagation only. For both radars, we have considered the period 2002–2004 to assess not only the diurnal cycle, but also the spatial differences.

The overall behavior of the daily evolution of the anaprop occurrence is shown in Figs. 2a and b. In these figures, the average percentage of cells affected by anaprop clutter for each hour over the whole radar domain is represented, considering the central months of the different seasons.

In either statistics, both a daily cycle and an annual cycle are clearly present. Starting with the annual behavior, summer shows the highest incidence of anaprop, with an affected mean area greater than 8%, and following spring, fall and winter show, in this order, fewer incidences.

The diurnal cycle in summer, spring and fall is similar, showing the highest incidence in the evening and in the first hours of the night, a secondary maximum during the central hours and two minima, the first around the 06:00 UTC and the latter 10 to 12 h later. This confirms previous studies using spatial classifications (Moszkowicz et al., 1994) and statistical analysis of radiosounding data in the Mediterranean area (Alberoni et al., 1998; Bech et al., 2002).

The SPC analysis highlights that the warmer the season the later the anaprop maximum is achieved: 22:00 UTC during summer, 20:00 UTC in spring and fall and 19:00 UTC in winter. This behavior is also present at GAT, with only smaller differences in the time occurrences. This suggests that these anaprop maxima are caused by the ascent of the nocturnal thermal inversion which, under clear skies and absence of significant air-mass changes, typically forms and deepens in the early evening hours, after sunset, as a result of radiative and sensible heat flux divergence (Arya, 1988).

The SPC diurnal cycle is smoothed in winter and in GAT seems to be inverted, with the minimum after the sunset in the evening. A secondary maximum, for both radars, is in the central part of the day, maybe associated to air convection circulation.

However, for SPC area, midnight conditions seem more similar to the previous hours respect to the following; instead, for the GAT area, the capability of 00:00 UTC observations to represent the subsequent propagation conditions, decreases less rapidly (like 12:00 UTC observation).

In order to analyze local variations due to the different environment in which radar beam propagates, a deeper analysis has been carried out comparing two cells or boxes for the SPC radar. The areas selected are representative of the coastal and the inland environments (refer to Fig. 1b for boxes placement). It is well evident that a larger AP presence occurs in the flat inland area during summer and during the other seasons, even if with smaller relative increase (Figs. 2c, d). This is likely to be an effect of the sea breeze circulation that is often present in the coastal area that, increasing the mixing of the surface layer, reduces the vertical gradient of refractivity.

The difference between the two radar statistics is well documented from the AP cycle in the common cell (Figs. 2e, f) shown in Fig. 1a. While on one hand the overall behavior of both radar is the same a more deep analysis reveals some differences. Focusing on the diurnal cycle SPC shown a relative highly frequency of AP during the night hours, this is existent in any season. The explanation of this effect is not so trivial. Since we are looking to the same area the atmospheric propagation conditions of the area are not the driving factors, these have to search in the propagation condition close to each radar site. We infer that local propagation conditions are influenced by differences in local orography. A larger presence of mountains in Gattatico area, leads to higher variability in horizontal refractivity gradient; in San Pietro Capofiume area, the higher incidence of anaprop, is probably due to advection of humid and cool air from the sea. Further Gattatico radar site is closer to the Apennine ridge respect the San Pietro Capofiume site, with a stronger valley breeze circulation. This effect is not so visible in Figs. 2a and b could be that, there, it is shown a combination of the "diurnal" and of the "seasonal" effects over the whole radar domain.

These results, providing a good description of the major features of seasonal and diurnal cycles, should be taken as a first approximation to the local climatology of anaprop.

4 Datasets for refractivity gradient retrieval

The Eq. (3) is derived under the hypothesis of a spherical stratified atmosphere, i.e. under the assumption that horizontal variation of the refractivity profile is negligible. Under this assumption, radiosounding data can be identified as the optimum dataset to represent the propagation conditions, because they have a very fine vertical resolution.

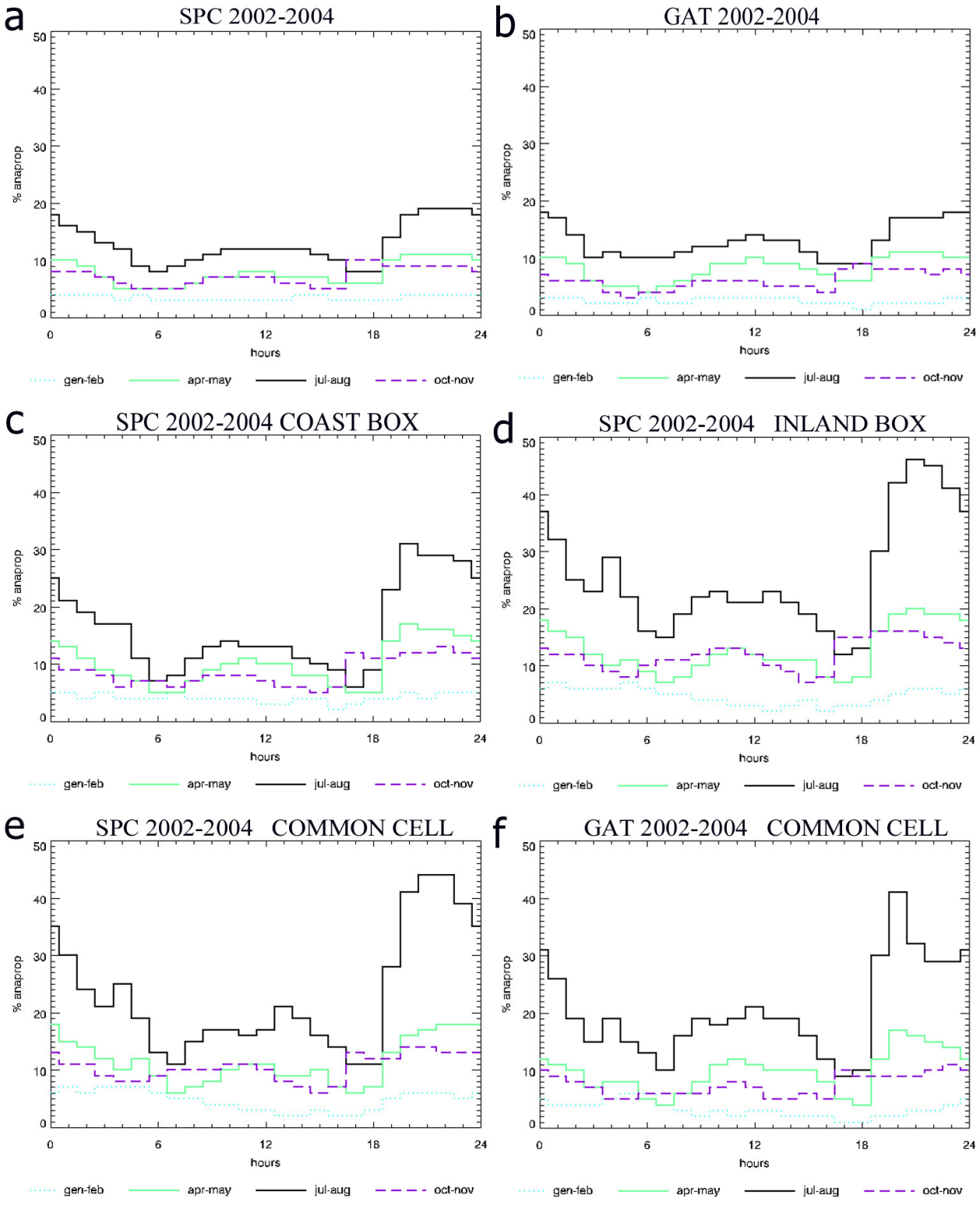

Fig. 2. Mean percentage of anaprop clutter detected. The average is calculated for each hour during the time range 1 January 2002–31 December 2004 for San Pietro Capofiume and for Gattatico radar. **(a)** Whole radar domain for SPC. **(b)** same as (a) for GAT. **(c)** Same as (a) for the coast area. **(d)** Same as (a) for the inland area. **(e)** Same as (a) in the common cell for SPC. **(f)** Same as **(e)** for GAT.

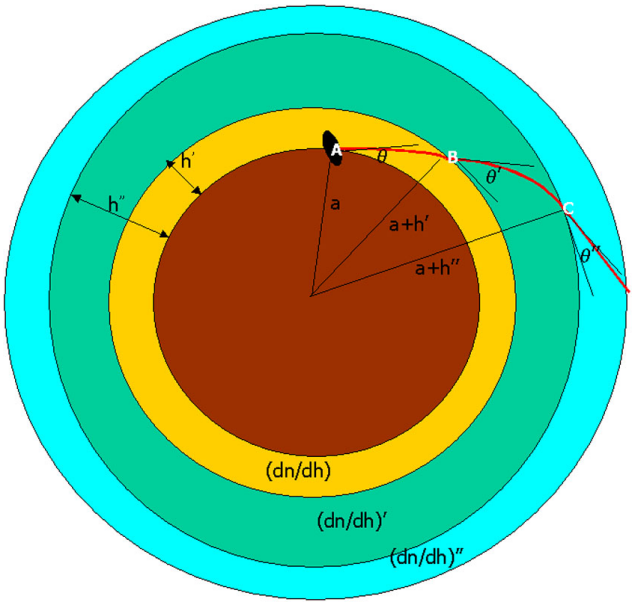

Fig. 3. The "layer by layer" ray tracing. A represents the radar site, B and C are point of intersection beam centre-layer. θ, θ_1, θ_2 are angle of interception ray-layer. h′ and h″ are heights of the layers base levels respect to radar level. dn/dh, dn/dh′, dn/dh″, represent the mean refractivity gradients into the three layers, a is the earth radius.

But in some cases, as stated before, the propagation may depend strongly on local thermodynamic conditions, which substantially vary in space and time; this is frequent in the land-sea interface and in complex orography terrain, as discussed by Hsu (1988) and Skolnik (2001). As a consequence, a sounding station is not generally able to characterize the propagation conditions over the whole radar domain; even if at particular point provides a high vertical resolution description. In order to address this problem, it has been tested the usefulness of the Lokal Model forecasts to predict the refractivity, comparing the profile extracted from the model with that extracted from radiosonde observation over the same point.

The radiosonde station is located at the SPC radar site and launches a sonde every twelve hours (00:00 UTC and 12:00 UTC). During the flight, data are collected every two seconds with an ascent rate of approximately 300 m/min, i.e. the maximum resolution is approximately 10 m. Radiosonde data are available at the original resolution (hereinafter RAW data), and in the FM 35 or TEMP format, according to the World Meteorological Organisation (WMO) standard data format commonly used for international exchange.

Lokal Model (LM) is a non-hydrostatic NWP model operational at ARPA-SIM (Bologna, Italy). It provides, every 3 h, pressure, temperature and humidity profiles, over a geographical domain covering the studied area, with a grid resolution of 7 km and 35 vertical levels and in strategic points such as sounding stations. For our analysis we have used LM data obtained from the nearest runs to the selected case study.

RAW data has been used as the reference dataset, in seven study cases, to evaluate the usefulness of TEMP and LM data, which are preliminarily interpolated at steps of 25 m. The comparison has been also extended to TEMP data, which are commonly available in meteorological applications. The N profiles have been calculated using Eq. (2).

5 A multi-layer ray-tracing model

In order to evaluate the differences in the beam path reconstruction using the three datasets available, a multi-layer propagation model has been implemented, i.e. an algorithm that takes into account the vertical variation of the refractivity gradient in the ray tracing. A single layer is characterized by a constant refractivity gradient.

To calculate the ray path, Eq. (3) has been used iteratively moving the origin of the calculation to the point of intersection between the ray and the layer and changing the refractivity gradient, as shown in Eq. (4):

$$h = \sqrt{r_l^2 + (k_{el}\ (a + H_l)^2 + 2 r_l k_{el}(a + H_l)\sin\theta_l} - k_{el}(a + H_l) + H_l \tag{4}$$

where the index l means "relative to the layer l"; consequently r_l is the distance from the new origin, H_l is the height of the layer l, k_{el} is the factor k_e for the layer l and θ_l is the angle of interception ray-layer. θ_g is calculated using the formula reported in Doviak and Zrnic (1993), modified for a generic number of layers and including the ducting case (if the beam bends to the ground, θ_g becomes negative):

$$\theta_l \cong \tan^{-1}\{ \pm \left[(a + H_{l-1})^2 \sin^2\theta_{l-1} + 2(a + H_{l-1})h_{l-1} (1 + (a + H_{l-1})(dn/dh)_{l-1})\right]^{1/2} / (a + H_{l-1})\cos\theta_{l-1}\} \tag{5}$$

where $h_{l-1}$is the thickness of the layer crossed (negative if the path is bent to the ground, as the root square). The final path is obtained connecting the different trajectories at each layer (see Fig. 3).

Finally, to describe qualitatively the power distribution within the beam we have represented an ensemble of numerous "elementary" rays with different initial angles. Particular attention has been devoted to the path of the 3-dB beam (centre and lower and upper limits).

6 Application on different case studies

As stated before, the summer season, mainly during night time, has the highest anaprop incidence. Therefore, 8 events of the summer 2003 have been selected for the analysis (7 correspond to the month of July, and the other one to June). Four of them are discussed here in more detail. For each case, in Fig. 4 is represented the refractivity gradient calculated in

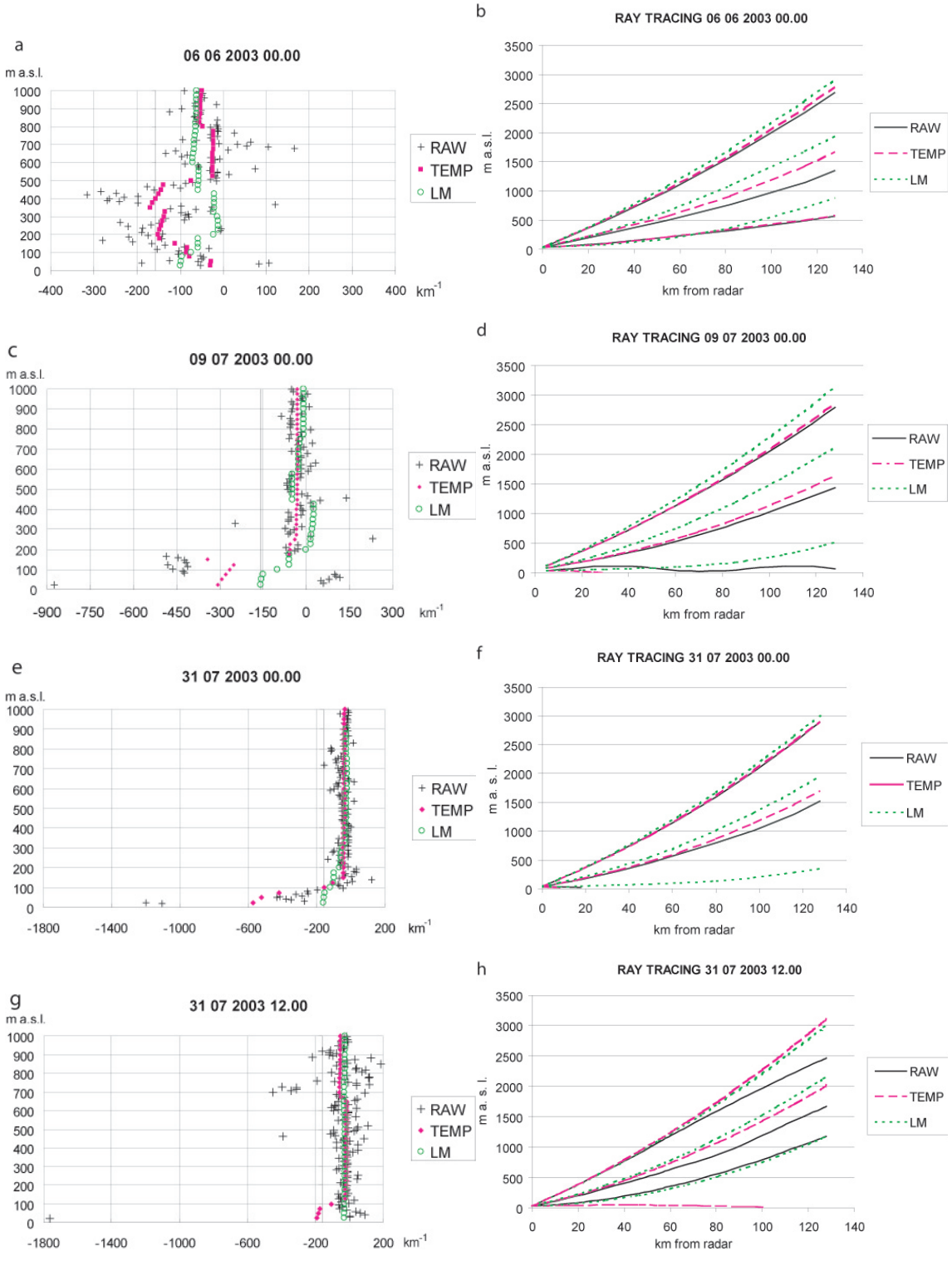

Fig. 4. **(a)** 6 June 2003, 00:00 UTC. Refractivity gradient profile obtained using RAW; TEMP and LM data. Note that the abscissa scale is not constant to highlight, where possible, the variability of the refractivity gradient. The vertical axis intercepts the refractivity gradient axis on the –157 km^{-1} value to evidence superrefraction conditions (−157 N/km is the threshold between superrefraction and ducting). **(b)** 6 June 2003, 00:00 UTC. Propagation path of the center, lower and upper limit of the 3 dB beam, at 0.5°elevation, for the RAW, TEMP and LM data. **(c)** as (a) for 9 July 2003, 00:00 UTC. **(d)** as b) for 9 July 2003, 00:00 UTC. **(e)** as (a) for 31 July 2003, 00:00 UTC. **(f)** as (b) for 31 July 2003, 00:00 UTC. **(g)** as (a) for 31 July 2003, 12:00 UTC. **(h)** as (b) for 31 July 2003, 12:00 UTC.

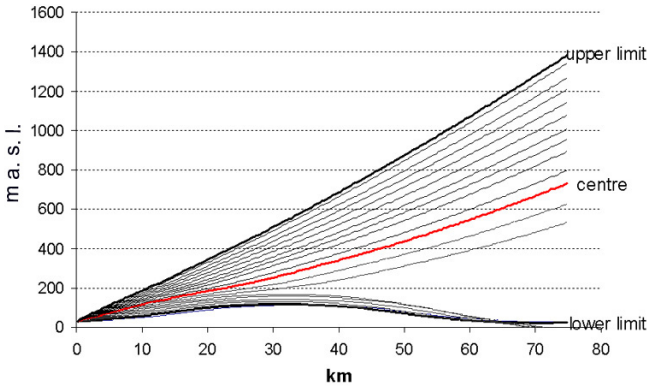

Fig. 5. Beam "splitting" on 9 July 2003 at 00:00 UTC. Power path has been represented dividing the beam in numerous shares and following the trajectory of each one. Near to the lower limit some trajectories intersect mutually.

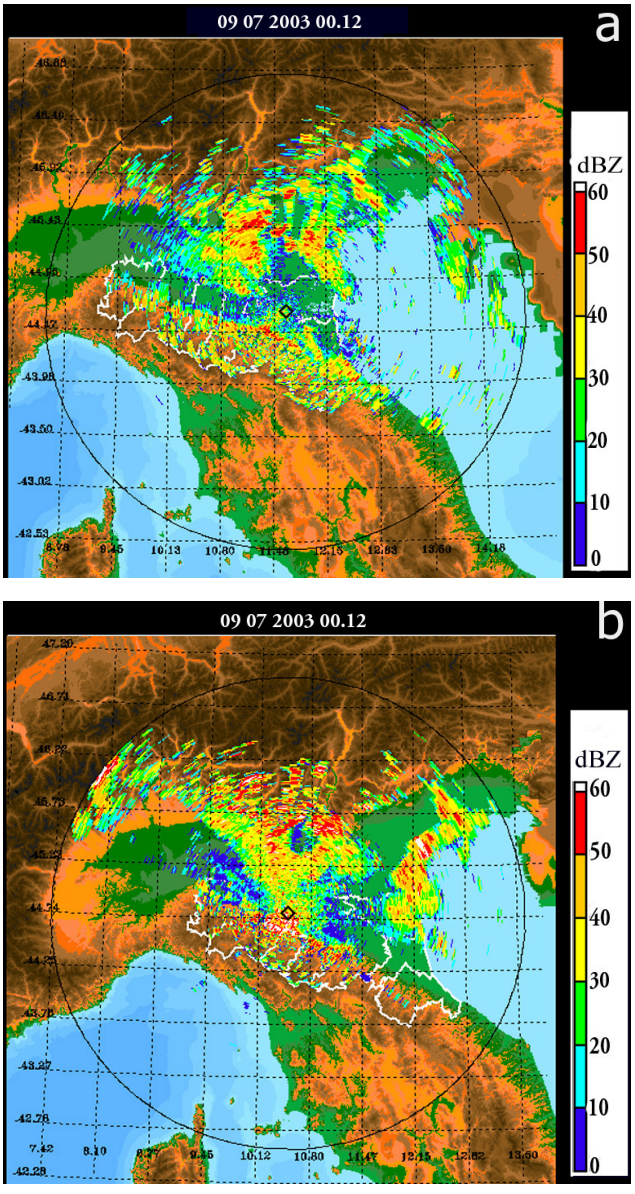

Fig. 6. 9 July 2003, 00:12 UTC Reflectivity maps; data are kept at the scan elevations of the static map. The white lines are boundaries of Emilia Romagna region. **(a)** SPC. **(b)** GAT.

the first km of atmosphere, over the SPC site, using RAW, TEMP and LM data and the correspondent beam path for each event (a, c, e, g and b, d, f, h, respectively).

The first day, 6 June 2003, is a fair weather day in Emilia Romagna region. RAW data show two elevated layers of superrefraction followed by a subrefraction layer around 700 m height, Fig. 4a. This strong vertical variability, which has been captured by the RAW data, is not well reproduced by the other datasets. TEMP data reproduce the profile tendency, but smoothed it, with a consequent quite deep layer (400 m depth) where the propagation is close to be superrefractive. The LM profile has difficulties to reproduce these features, though simulates correctly a superrefractive surface layer. It is worth to be noted that above the 700 m the propagation is very close to the standard one. The ray-tracing simulation is shown in Fig. 4b. The path of the lower limit is conditioned by the first layer of superrefraction; it is well reproduced with the TEMP data but not with LM data, where the structure is completely absent. The path of the centre is conditioned by the second layer of superrefraction and is not well reproduced neither by TEMP nor LM data. Indeed, while for the first the smoothing prevents the occurrences of the stronger effect, for the latter the profile does not show the feature at all. Finally, the upper path is well reproduced by all datasets: as pointed out previously, the propagation effects are most prominent at lower elevations. These discrepancies give a different distribution of the power density in the three cases and different observed volumes. For example, TEMP and RAW observed volumes are larger than LM; the power density in the lower part of RAW beam is higher than in the upper part.

The 9 July 2003, 00:00 UTC (Fig. 4c), another fine weather day in Emilia Romagna, the refractivity profile shows subrefraction in the first 100 m (except the surface layer), followed by a very marked ducting layer with values around $-450\,\mathrm{km}^{-1}$ up to 200 m and beyond standard conditions. TEMP data smooth the superrefraction and are not able to identify subrefraction in the lowest layers, LM data reproduce the ducting layer but also smoothed. As a consequence (Fig. 4d), the TEMP lower path reaches the ground approximately at 30 km distance from the radar site, RAW lower path oscillates with a wave length of 75 km and a vertical amplitude of 100 m, the LM lower path is not trapped but it is below the standard trajectory (the standard refraction trajectory has a height of nearly 1000 m at 125 km). The centre path is not well reproduced by TEMP and LM data. In the RAW data, the power density distribution oscillates with the distance, as the observed volume. Moreover, to describe better

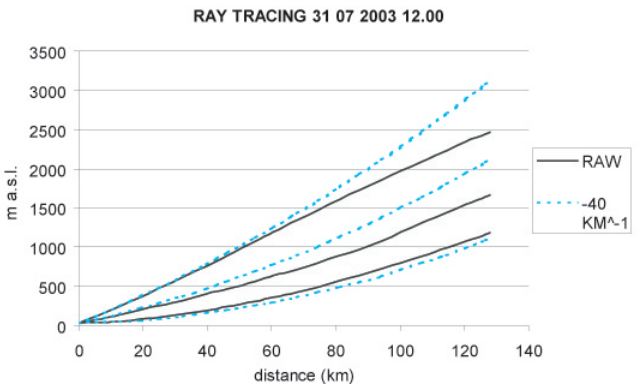

Fig. 7. Comparison between the 3-dB beam shapes calculated using RAW data and standard propagation conditions, on the 31 July 2003 at midday. The three lines represent lower limit, centre and upper limit of a 1° beam.

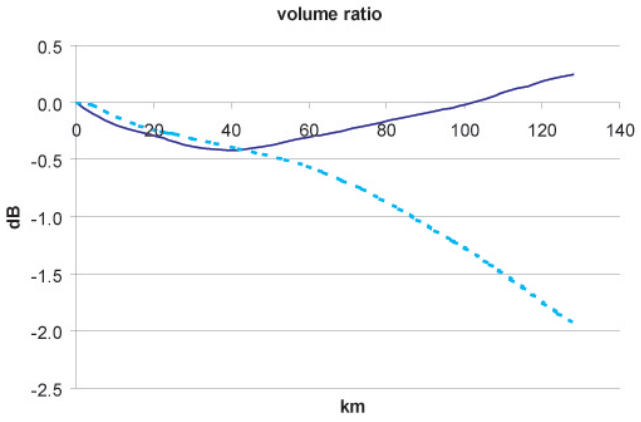

Fig. 8. Ratio between the 3-dB observed volume calculated using standard propagation and that obtained from RAW data, in the 6 June 2003, 00:00 UTC and the 31 July 2003, 12:00 UTC cases with superrefaction but without ray trapping.

the propagation of the 3 dB main lobe, the paths of a higher number of elementary rays have been plotted in Fig. 5, in order to remark the different behavior of their trajectory. It may be clearly appreciated that at a range of approximately 30 km, the rays are separated into two different groups splitting the beam in two lobes. This effect is known as beam-splitting and implies the existence of a region, which remains unexplored, known as "radio hole". In this particular example, the radio hole is the layer centred at an altitude of 200 m starting at 30 km from the radar. Beam–splitting is very important in military applications because target detection and communication in radio holes may be completely impossible. For weather radars, beam–splitting distorts drastically the integration volume assumed in normal propagation conditions making very difficult to retrieve the real density distribution and the observed volume (in this case even some ray trajectories intersect making the calculation even more complex). The oscillation related to the trapping layer is visible in the reflectivity map of San Pietro Capofiume (Fig. 6a) as clutter "rings"; this phenomenon is also described by Bebbington (1998) and Gerstoft et al. (2000); further, the splitting causes a sort of strike effect due to the shadow of some mountains north of the radar. On the GAT radar the severe propagation conditions are also present and a conspicuous amount of anaprop echo is present (Fig. 6b); it should be noted, in this image, the reflectivity 'hole' produced by the Garda lake north of the radar site.

On the 31 July 2003 are present anaprop and some convective cells, on the mountains, after midday. The profile (Fig. 4e) at 00:00 UTC is quite regular showing a deep superrefraction layer in the first 100 m that produces ducting, indeed the 3 dB beam lower limit reaches the ground after only 20 km (Fig. 4f). The TEMP data reproduce quite accurately this trend, while LM data are not able to recognize the ducting, even if a condition of superrefraction is identified. For this reason, the beam path based on LM does not touch the ground.

The situation changes at 12:00 UTC. The surface duct is completely disappeared and an elevated (700–800 m) superrefraction layer is present (Fig. 4g). The surface N gradient (19–27 m) is extremely strong, approximately −1700 km, but the following values show mainly normal refraction. The TEMP profiles, which are interpolated with the hypsometric equation, conserve too long the influence of the first point, producing a false ducting layer. LM data produce only normal refraction conditions. Consequently, the lower limit path is more similar to that produced by LM data than the one produced by TEMP data. The elevated superrefraction layer produces an additional bending of the path that is not recognized by TEMP and LM data (Fig. 4h). In this case, the observed volume (as the power distribution) is very different from those defined by TEMP and LM, and also from standard conditions geometry, as is represented in Fig. 7.

In this condition the beam vertical broadening θ' is less than in standard propagation (θ) and this produces an increase in the gain, which is proportional to the ratio between the standard and current width: the same power is in fact distributed on a smaller solid angle. If we assume that the power density increases homogeneously, calling g_M and g'_M the maximum gain in standard propagation and in the current propagation conditions, we have:

$$\theta'_{3dB} = \frac{1}{a}\theta_{3dB} \tag{6}$$

$$g'_M = a \cdot g_M \tag{7}$$

The received power is proportional to the following term (see Doviak and Zrnic, 1993):

$$g^2 M' \cdot \int_{4\pi} f'^4(\theta, \varphi) d\Omega \tag{8}$$

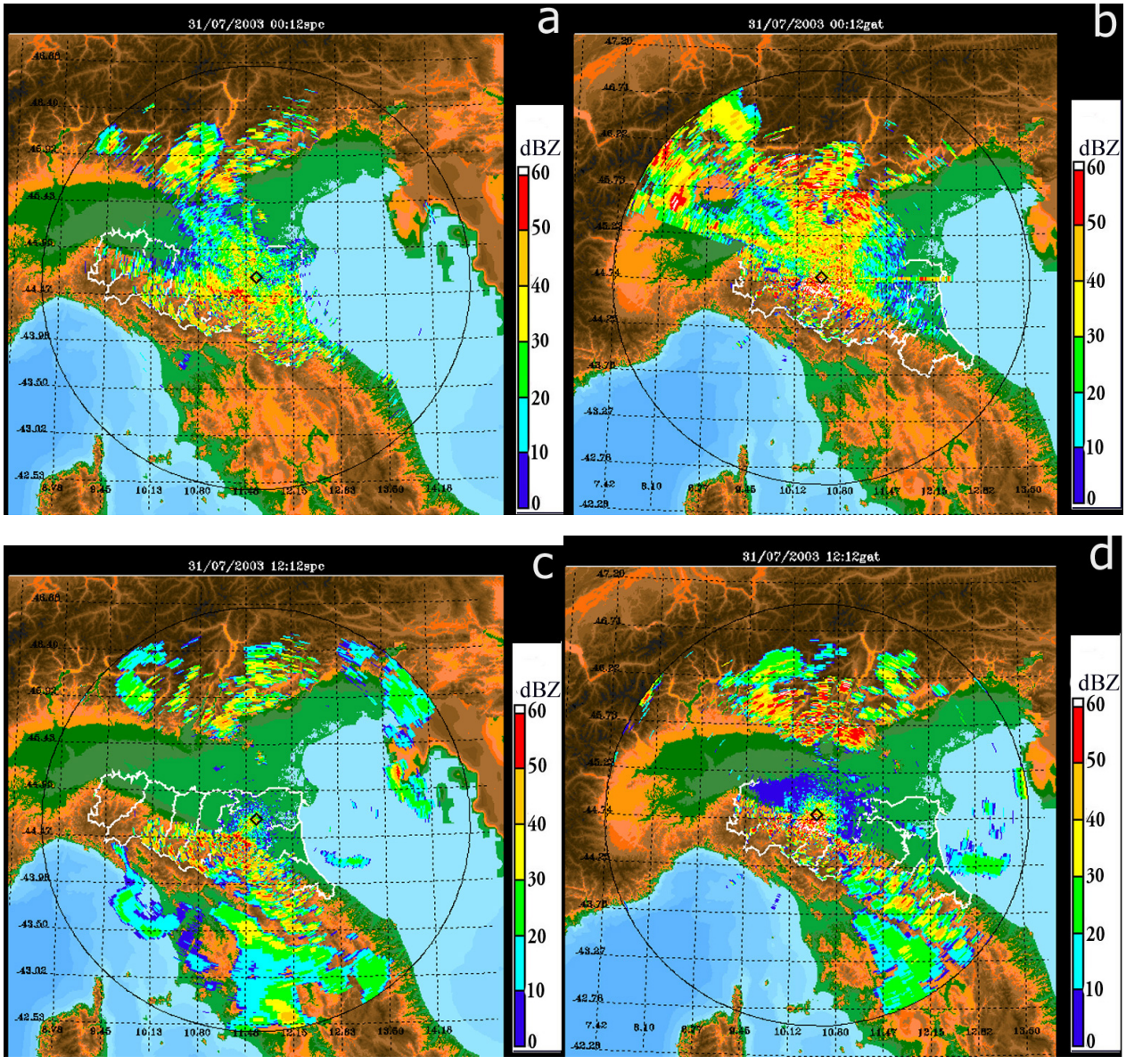

Fig. 9. a) As Fig. 6a for the 31 July 2003 00:12 UTC, **(b)** as **(a)** for GAT. **(c)** As (a) at 31 July 2003, 12:12 UTC. **(d)** as **(c)** for GAT.

Using the integral solution of the radar equation (Probert-Jones, 1962)

$$\int_{4\pi} f'^4(\theta,\varphi)d\Omega = \frac{\theta'_{3dB}\varphi_{3dB}}{8\ln 2}\pi = \frac{1}{a}\int_{4\pi} f^4(\theta,\varphi)d\Omega \qquad (9)$$

where $f(\theta s\varphi)$ and $f'(\theta s\varphi)$ are the gaussian functions of power density distribution, the received power P'_r increases of a factor a.

$$P'_r = a \cdot P_r \qquad (10)$$

Usually, the power reaching the target and the integration volume are calculated considering standard propagation conditions (i.e. the angular amplitude is approximately constant); therefore, in these cases, an error may be introduced.

Assuming that, within the beam, the power distribution remains gaussian, the use of standard propagation produces an error in the reflectivity retrieval equal to the difference between the volume observed and the volume assumed in standard conditions (see Fig. 8). The error due to incorrect volume definition reaches nearly 2 dB in the case study of 31 July; in others, such as the 6 June, this effect is almost negligible (an error lower than 0.5 dB). If the gaussian distribution cannot be assumed reliably, in particular when the power is "splitted", then the problem becomes more complex and is not considered here.

Finally, it is interesting to observe the reflectivity maps of SPC and GAT in the two latter cases. As described from the ray tracing, at midnight (Figs. 9a, b) the beam bent to the ground after some kilometres: the clutter echo in GAT and SPC is continuous (the echo of secondary lobes is added to the one produced by the main lobe). At midday in SPC area (Fig. 9c) clutter is observed only in mountainous terrain (except the secondary lobes). This fact confirms the ray tracing modelling: the beam height is lower but there is no ducting. GAT observations (Fig. 9d) are somewhat different: probably a more marked superrefraction layer is present because the clutter area around the radar is very large. This confirms the higher horizontal variability of the refractivity gradient over complex orography terrain.

7 Conclusions

An analysis of the anaprop occurrences in the Po Valley (Italy) has been carried out based on radar data. The outcomes of this analysis confirm what was previously observed using a complete different approach based on sounding observations in the same area, but in a different period. This enforces the result found.

An annual cycle is present with a clear maximum during the warmer season. Further, the onset of anaprop presence shows a well defined diurnal cycle. This is a possible clear indication on when data are prone to be affected by the propagation effects.

The anomalous propagation conditions have been examined in representative cases, using different datasets to retrieve refractivity profiles. Their relative capabilities to reproduce the beam path and shape have been also discussed.

It has been noted that, in general, a high variability of the refractivity gradient occurs in the first 300 m, where most part of ducting effects take place; above 500–600 m the mean profile is more regular, as presented by the RAW dataset. The TEMP output reproduces quite well the mean profile of N, but not its variability, which plays a fundamental role in the propagation of the radar beam. However, TEMP data can introduce superrefraction in normal conditions, if the second point of measure is far from the ground point. The main problem of this type of data is to accurately detect super- and subrefraction layers and to determine its thickness. The Numerical Weather Prediction Lokal Model data is inadequate to predict either the N gradient variability or the mean N gradient in the first 200–300 m, even if it detects some "suspect" situations; i.e. it can predict superrefraction conditions but not its magnitude and thickness, that is systematically underestimated.

Observing the ray tracing of the centre and lower and upper limits and of the main lobe beam, we have concluded that ducting layers produce a change in the measured volume and in the power distribution that can lead to an additional error in the reflectivity estimate. This error can be present even in absence of anaprop clutter and can reach significant values in extreme cases. However, the 3-dB beam observed volume is difficult to retrieve in cases of ducting, because the trajectories of rays at very low elevations can intersect and the beam becomes splitted.

Acknowledgements. This work is partially supported by CARPE DIEM, a research project supported by the European Commission under the 5th FP (Contract N° EVG1-CT-2001-0045), and by the INTERREG IIIB programme through the RISK AWARE project (Contract N° 3B064). We gratefully acknowledge two anonymous reviewers who helped to improve the clarity and content of this paper.

Edited by: L. Ferraris
Reviewed by: K. Commins and another referee

References

Alberoni, P. P., Anderson, T., Mezzasalma, P., Michelson, D. B., and Nanni, S.: Use of the vertical reflectivity profile for identification of anomalous propagation, Meteorol. Appl., 8, 257–266, 2001.

Alberoni, P. P., Nanni, S. Mezzasalma, P., Bech, J., Lorente, J., and Codina, B.: Dynamic suppression of anaprop conditions, Final report to the European Union on contract No. ENV4-CT96-0261, "DARTH Project", 1998.

Alberoni, P. P., Ducrocq, V., Gregoric, G., Haase, G., Holleman, I., Lindskog, M., Macpherson, B., Nuret, M., and Rossa, A.: Quality and Assimilation of Radar Data for NWP–A Review, COST 717 document, ISBN 92-894-4842-3, 38, 2003.

Arya, S. P.: Introduction to Micrometeorology, Academic Press, Inc., 307, 1988.

Babin, M. S.: Surface duct height distribution for Wallop Island, Virginia, 1985–1994, J. Appl. Meteorol., 35, 86–93, 1996.

Bean, B. R. and Dutton, E. J.: Radio Meteorology, Dover Publications, 435, 1968.

Bebbington, D.: DARTH EU Project Final Report, Part II, Anomalous, Propagation Modelling, Essex University, UK, 18 , 1998.

Bech, J., Codina, B., Lorente J., and Bebbington, D.: Monthly and daily variations of radar anomalous propagation conditions: How "normal" is normal propagation?, Proceedings of the 2nd European Meteorological Radar Conference, Delft, Netherlands, 35–39, 2002.

Bech, J., Codina, B., Lorente, J., and Bebbington, D.: The sensitivity of single polarization weather radar beam blockage correction to variability in the vertical refractivity gradient, J. Atmospheric and Oceanic Technology, 20, No 6, 845–855, 2003.

Bech, J., Toda, J., Codina, B., Lorente, J., and Bebbington, D.: Using mesoscale NWP model data to identify radar anomalous propagation events, Proceedings of the 3rd European Meteorological Radar Conference, Visby, Sweden, 310–314, 2004.

Doms, G. and Schaettler U.: The non-hydrostatic Limited-Area Model LM (Lokal Modell) of DWD. Part I: Scientific documentation, Deutscher Wetterdienst (DWD), Offenbach, 1999.

Doviak, R. J. and Zrnic, D. S.: Doppler radar and weather observations, Academic Press, 9–18, 1993.

Gerstoft, P., Rogers, L. T., Wagner, L. J., and Hodgkiss, W. S.: Estimation of radio refractivity structure using matched field ar-

ray processing, IEEE J. Antenna and Propagation, 48, 345–356, 2000.

Hsu, S. A.: Coastal meteorology, Academic Press, 260, 1988.

ITU: The radio refractive index: Its formula and refractivity data, ITU-R P-Series, Doc. ITU-R P.453-6, ITU Radiocommunication Assembly, 9, 1997.

Moszkowicz, S., Ciach, G. J., and Krajewski, W. F.: Statistical detection of anomalous propagation in radar reflectivity patterns, J. Atmos. Oceanic Technol., 11, 1026–1034, 1994.

Probert-Jones, J. R: The radar equation in meteorology, Q. J. R. Meteorol. Soc., 88, 485–495, 1962.

Raghavan, S.: Radar Meteorology (Atmospheric and Oceanographic Sciences Library, 27), Kluwer Academic Publishers, 59–61, 2003.

Skolnik, M. L: Introduction to radar Systems, 3rd edition, Mc Graw Hill, 2001, 494–518.